

LETTER TO THE EDITOR

“TNOs are Cool”: A survey of the trans-Neptunian region^{*}

I. Results from the *Herschel* Science Demonstration Phase (SDP)

T. G. Müller¹, E. Lellouch², J. Stansberry³, C. Kiss⁴, P. Santos-Sanz², E. Vilenius¹, S. Protopapa⁵, R. Moreno², M. Mueller⁶, A. Delsanti^{2,7}, R. Duffard⁸, S. Fornasier^{2,9}, O. Groussin⁷, A. W. Harris¹⁰, F. Henry², J. Horner¹¹, P. Lacerda¹², T. Lim¹³, M. Mommert¹⁰, J. L. Ortiz⁸, M. Rengel⁵, A. Thirouin⁸, D. Trilling¹⁴, A. Barucci², J. Crovisier², A. Doressoundiram², E. Dotto¹⁵, P. J. Gutiérrez⁸, O. R. Hainaut¹⁶, P. Hartogh⁵, D. Hestroffer¹⁷, M. Kidger¹⁸, L. Lara⁸, B. Swinyard¹³, and N. Thomas¹⁹

(Affiliations can be found after the references)

Received November 10, 2018; accepted

ABSTRACT

The goal of the *Herschel* Open Time Key programme “*TNOs are Cool!*” is to derive the physical and thermal properties for a large sample of Centaurs and trans-Neptunian objects (TNOs), including resonant, classical, detached and scattered disk objects. We present results for seven targets either observed in PACS point-source, or in mini scan-map mode. *Spitzer*-MIPS observations were included for three objects. The sizes of these targets range from 100 km to almost 1000 km, five have low geometric albedos below 10%, (145480) 2005 TB₁₉₀ has a higher albedo above 15%. Classical thermal models driven by an intermediate beaming factor of $\eta=1.2$ or η -values adjusted to the observed colour temperature fit the multi-band observations well in most cases. More sophisticated thermophysical models give very similar diameter and albedo values for thermal inertias in the range $0\text{-}25\text{ J m}^{-2}\text{ s}^{-0.5}\text{ K}^{-1}$, consistent with very low heat conductivities at temperatures far away from the Sun. The early experience with observing and model strategies will allow us to derive physical and thermal properties for our complete *Herschel* TNO sample of 140 targets as a benchmark for understanding the solar system debris disk, and extra-solar ones as well.

Key words. Kuiper belt – Infrared: solar system – Techniques: photometric

1. Introduction

Trans-Neptunian objects (TNOs) are believed to represent one of the most primordial populations in the solar system (Morbidelli et al. 2008). The TNO population comprises (i) the main Kuiper belt beyond the orbit of Neptune ($\sim 32\text{ - }50\text{ AU}$), consisting of objects in resonant and non-resonant orbits, and (ii) the halo outskirts of “scattered” and “detached” bodies beyond 50 AU. The Centaurs, an unstable orbital class of minor planets (e.g., Horner et al. 2003; 2004), are closer to the Sun and in transition from the Kuiper belt towards the inner solar system. More than 1300 TNOs have been detected so far, revealing a rich orbital structure and intriguing physical properties. The Trans-Neptunian population is analogous to the debris disks observed around several other, 5-500 Myr old stars (Moro-Martín et al. 2008, Jewitt et al. 2009). This analogy is bolstered by similarities in sizes and observed masses (typically 30-300 AU and $0.01\text{-}0.1 M_{\oplus}$ for the “exo-disks”), with the important difference that the detected mass in extra-solar debris disks is in the form of $\sim 10\text{-}1000\text{ }\mu\text{m}$, short-lived, dust particles. The vast majority of the mass in these disks is invisible to us, probably in the form of kilometre (or more)-sized bodies, resembling trans-Neptunian objects.

As part of the *Herschel* (Pilbratt et al. 2010) Science Demonstration Phase we observed 17 targets in different instrument configurations and observing modes. Here we present the analysis of early photometric measurements with

the Photodetector Array Camera and Spectrometer (PACS - Poglitsch et al. 2010) of five TNOs and two Centaurs. The science aspects from longer wavelengths Spectral and Photometric Imaging Receiver (SPIRE - Griffin et al. 2010) observations on (136472) Makemake and (90482) Orcus are included in Lim et al. (2010) and the thermal lightcurve of (136108) Haumea is presented by Lellouch et al. (2010). The full Open Time Key Programme includes about 140 TNOs (Müller et al. 2009).

2. Observations and data reduction

The PACS photometric measurements (70/100/160 μm bands) were either taken in point-source mode with chopping-nodding on three dither positions (pre-launch recommended mode for point-sources), or in mini scan-map mode covering homogeneously a field of roughly $1'$ in diameter (Poglitsch et al. 2010). The mini scan-map mode turned out to be more sensitive and better suited for our project.

The chop-nod data reduction was done in a standard way (Poglitsch et al. 2010). The scan map processing deviated from the default way: Two scans were joined (for combined scan-maps) before executing first an unmasked high-pass filtering to identify sources and bright regions, which were then masked for a second high-pass filtering (without deglitching on the masked sources). The filter widths of the high pass were empirically chosen to be $62''$ and $82''$ in for the 70/100 μm maps and 160 μm maps, respectively, for S/N and flux conservation reasons. Then second order deglitching was applied in the source regions and the final maps were created. The calibration was done by apply-

^{*} *Herschel* is an ESA space observatory with science instruments provided by European-led Principal Investigator consortia and with important participation from NASA.

Table 1. Observation summary: target name, observation identifier from the *Herschel Science Archive* (OBSID), observation mid-time (UT) in 2009, observation duration [s], mode: chopping/nodding/dithering or map parameters for 20''/s mini scan-map mode (scan leg length, separation, number of scans, map orientation in detector array-coordinates), repetition factor either for a chop-nod cycle or for full map, PACS photometer bands, colour-corrected flux values at PACS photometer reference wavelengths λ_c : 70 or 100, as well as 160 μm .

Target	Obs. ID	Mid-time [UT]	Dur. [s]	Mode/Remarks	Bands	FD [mJy]	
(208996) 2003 AZ84	1342187054	11-16 19:20	2526	chop/nod/dither/16	70/160	27.0±2.7	19.8±5.2
(126154) 2001 YH140	1342187062	11-17 18:37	5666	chop/nod/dither/36	70/160	9.8±2.9	<13
(79360) 1997 CS29	1342187073	11-18 14:24	5666	chop/nod/dither/36	70/160	5.1±1.2	14.5±2.9
(82075) 2000 YW134	1342187074	11-18 16:00	5666	chop/nod/dither/36	70/160	<5	<8
(42355) Typhon	1342187113	11-20 00:05	1584	chop/nod/dither/10	70/160	17.0±3.4	<13
	1342187114	11-20 00:33	1584	chop/nod/dither/10	100/160	16.4±1.9	<10
	7113&7114	11-20 00:19	3168	combined	160		<9
2006 SX368	1342188416	12-21 19:02	2722	3.5'/4.0''/10/ 63°/9	70/160	24.1±1.3	<15
	1342188417	12-21 19:49	2722	3.5'/4.0''/10/117°/9	70/160	26.4±5.8	<22
	8416&8417	12-21 19:26	5444	combined scan-maps	70/160	22.2±2.9	<17
(145480) 2005 TB190	1342188482	12-23 20:08	2722	3.5'/4.0''/10/ 63°/9	100/160	4.6±0.7	<7
	1342188483	12-23 20:55	2722	3.5'/4.0''/10/117°/9	100/160	5.5±0.8	3.6±1.5
	8482&8483	12-23 20:24	5444	combined scan-maps	100/160	4.7±0.6	<6

ing flux overestimation corrections of 1.05, 1.09 and 1.29 at 70, 100 and 160 μm , as recommended in the PACS release note on point-source photometry¹.

In order to obtain monochromatic fluxes at the reference wavelengths 70, 100 and 160 μm we applied colour corrections of 0.98, 0.99 and 1.01 (Poglitsch et al. 2010), with uncertainties of approximately $\pm 1\%$ related to the full range of possible TNO and Centaur colour temperatures. The photometry of the targets was done by applying a standard technique, described in Lellouch et al. (2010). Table 1 summarises the selected SDP PACS observations with relevant instrument and satellite parameters together with the obtained fluxes. The monochromatic fluxes are listed with 1σ -errors, including also systematic errors like sky background gradients and variations. For non-detections we gave the 3σ errors as upper flux limits.

3. Observational results and model input parameters

In order to derive sizes and albedos from thermal-IR observations a thermal model is required. The thermal emission of an atmosphereless spherical body at distance Δ is given by

$$F(\lambda) = \epsilon R^2 / \Delta^2 \int \int B[T(\theta, \varphi)] \cos^2 \varphi \cos(\theta - \alpha) d\theta d\varphi \quad (1)$$

where ϵ is the emissivity, R the radius of the object, B the Planck function, φ the latitude, θ the longitude measured from the sub-solar point, and α the solar phase angle. As is usual for small bodies we adopt $\epsilon = 0.9$ throughout this work. The use of this equation requires a model of the temperature distribution $T(\theta, \varphi)$ over the surface. We applied the following models: (i) The standard thermal model (STM, Lebofsky et al. 1986), which describes a non-rotation, low thermal inertia surface in instantaneous thermal equilibrium with insolation (beaming parameter $\eta=0.756$, optimised for mid-IR colour temperatures of large main-belt asteroids); (ii) The fast rotating model or isothermal latitude model (FRM, ILM, Veeder et al. 1989, Lebofsky & Spencer 1989), as an extreme case of a high thermal inertia and/or fast rotating body; (iii) Intermediate models with respect

to STM and ILM, e.g., the near-Earth asteroid thermal model (NEATM, Harris 1998), where the beaming parameter η is fitted to the multi-band data ($T \propto \eta^{-1/4}$); (iv) A thermophysical model (TPM, Lagerros 1996, 1997, 1998; Müller & Lagerros 1998), where the temperature distribution is calculated for the given illumination and observing geometry, rotation axis and period have to be assumed if not available. The “free” parameter is the thermal inertia, a physical property of the surface material. The TPM assumes a “default” roughness (Müller & Lagerros 2002), while the η -driven models work with smooth surfaces.

Table 2 summarises the observing geometries, the H-magnitudes with absolute uncertainties, lightcurve influences and rotation periods which were used as input for the modelling. Effective diameter D_{eff} , geometric albedo p_V and H_V magnitude are connected via $D_{\text{eff}} = 1347.4 \times 10^{-0.2 H_V} / \sqrt{p_V}$ (Bowell et al. 1989). Knowing H_V (i.e., the reflected part of the Sun-light) and measuring fluxes at thermal wavelengths (i.e., the thermally re-emitted Sun-light) allows now to solve for D_{eff} and p_V , the effective diameter of the target and its geometric albedo. An uncertainty of 0.1 mag in H_V leads to errors of 4-5% in the derived diameter and 8-10% for the geometric albedo.

4. Results and discussion

The combined *Herschel* and *Spitzer* data show that neither of the “canonical” models (STM, ILM) fit the observed fluxes over the entire wavelength range (see Fig. 1 and Fig. 2). The data require either an intermediate beaming value η (or different ones for different parts of the SED) or a more sophisticated TPM with the thermal inertia Γ as key parameter for the temperature distribution on the surface. The value $\eta = 1$ corresponds to a smooth surface with zero thermal inertia. For our observations, which are carried out at low solar phase angle, thermal inertia would be expected to raise η (because it reduces the day-side temperature), while roughness leads to higher-than-expected effective temperatures, hence it lowers η . Both model techniques were applied. For the TPM we used a χ^2 -technique to find optimum solutions and uncertainties which are compliant with the observed fluxes and errors. The η -NEATM uncertainties are either based on a bootstrap Monte-Carlo analysis (e.g., Mueller et al. 2010) for the three targets where MIPS and PACS observations are available or on a fixed $\eta = 1.2 \pm 0.3$ in all other cases.

¹ PICC-ME-TN-036, 22/Feb/2010: herschel.esac.esa.int

Table 2. *Herschel* observing geometries for our seven targets, including properties derived from ground-based visible observations and the obtained radiometric solutions. r : Sun-target distance, Δ : *Herschel*-target distance, α : phase angle; H_V magnitudes, lightcurve Δ_{mag} , and the rotation period P ; references for the preceding three columns, derived effective diameter D_{eff}^{TPM} in [km] and geometric albedo p_V^{TPM} values from the TPM analysis, the corresponding possible thermal inertias Γ [$J m^{-2} s^{-0.5} K^{-1}$], and the fitted NEATM η value (*: for a fixed value).

Target	r [AU]	Δ [AU]	α [°]	H_V [mag]	Δ_{mag}	P [h]	Ref.	D_{eff}^{TPM}	p_V^{TPM}	Γ	η
2003 AZ ₈₄	45.376	44.889	1.11	3.83±0.04	0.14±0.03	6.79 h	1,2,3	850-970	0.05-0.09	2-10	1.31
2001 YH ₁₄₀	36.576	36.169	1.44	5.8±0.2	0.13±0.05	13.2 h	4	300-390	0.06-0.10	0-10	1.2*
1997 CS ₂₉	43.509	43.241	1.27	5.65±0.09	<0.08, <0.22	—	5, 6, 7, 8	250-420	0.06-0.14	0-25	1.2*
2000 YW ₁₃₄	44.125	43.833	1.25	4.88±0.05	<0.10	—	9, 10	<500	>0.08	0-25	—
Typhon	17.943	18.376	2.84	7.68±0.04	0.07±0.01	9.67 h	4, 11, 12	134-154	0.065-0.085	1-10	0.96
2006 SX ₃₆₈	11.972	12.271	4.48	9.5	—	—	MPC	70-80	0.05-0.06	0-40	1.2*
2005 TB ₁₉₀	46.377	46.683	1.17	4.58±0.22	0.12±0.02	12.68 h	13	335-410	0.15-0.24	0-25	1.2*

References: (1) Fornasier et al. 2004; (2) DeMeo et al. 2009; (3) Perna et al. 2010; (4) Thirouin et al. 2010; (5) Sheppard & Jewitt 2002; (6) Romanishin & Tegler 1999; (7) Davies et al. 2000; (8) Boehnhardt et al. 2001; (9) Sheppard & Jewitt 2003; (10) Doressoundiram et al. 2005; (11) Rabinowitz et al. 2007; (12) Tegler et al. 2003; (13) Thirouin et al. in prep.; MPC: <http://www.cfa.harvard.edu/iau/lists/Centaurs.html>

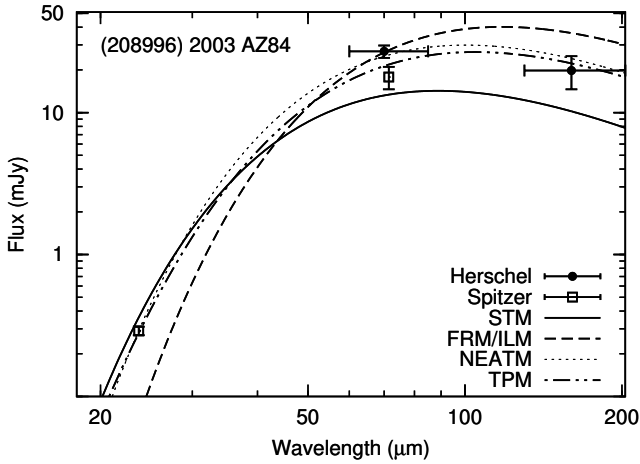


Fig. 1. Observed *Herschel* and *Spitzer* flux values for 208996 (2003 AZ84). This example illustrates that the simple “canonical” STM and FRM/ILM fail to match the full SED range. Either a model with floating η or a TPM is necessary for the observed TNOs.

(208996) 2003 AZ₈₄ is a Plutino in 3:2 mean-motion resonance (MMR) with Neptune with an eccentricity² of 0.18 and inclination of 13.5°. In combination with fluxes from Table 1 we used updated 24 and 70 μm MIPS fluxes from Stansberry et al. (2008) ($F_{24}=0.28\pm0.02$ mJy; $F_{70}=24.6\pm3.1$ mJy). The best η -based model solution resulted in an effective diameter of 896 ± 55 km and a geometric albedo of $p_V=0.065\pm0.008$, the corresponding beaming parameter is $\eta=1.31\pm0.08$. A more sophisticated TPM analysis on the basis of a spherical body with the given rotation period and a spin axis perpendicular to the solar direction, supported by a strong visible lightcurve (see Table 2), gave very similar D_{eff} and p_V values at a thermal inertia of $5^{+5}_{-3} J m^{-2} s^{-0.5} K^{-1}$. The very low thermal inertia is an indication that the surface might be covered by loose regolith with a low heat capacity in poor thermal contact. Although there are indications of crystalline water ice on the surface (Guilbert et al. 2009), a solid compact layer of ice can be excluded, because this would require significantly higher thermal inertia. It was also possible,

via the TPM, to investigate the influence of spin axis orientation, sense of rotation and rotation period, but for objects with very low thermal inertia the influence of the rotational properties are only on a level of less than 5% on the effective diameter and geometric albedo solutions. The diameter and albedo results agree with the Stansberry et al. (2008) values within the given error bars. The results of all model fits are shown in Fig. 1. The lightcurve influence (see Δ_{mag} in Table 2) is significant and has been taken into account (0.14 mag correspond to a $\sim 7\%$ diameter change and $\sim 14\%$ albedo change).

(126154) 2001 YH₁₄₀ is a dynamically hot object with a semi-major axis close to the 5:3 MMR with Neptune, which might have excited the orbit from a previously dynamically colder orbit. 2001 YH₁₄₀ was not observed by *Spitzer* and our PACS observation was done in chop-nod technique and with only a single epoch in the 160 μm band. Based on an assumed $\eta = 1.2\pm0.3$ the 70 μm detection leads to a NEATM-solution of $D_{eff}=349\pm81$ km and $p_V=0.08\pm0.05$. The result from the TPM analysis is similar with a possible diameter range between 300 and 400 km and geometric albedos between 0.05 and 0.10, based on a range of thermal inertias from 0 to $10 J m^{-2} s^{-0.5} K^{-1}$. These solutions correspond to predicted flux values of 6-11 mJy at 160 μm , compatible with the upper flux limit of 13 mJy at 160 μm .

(79360) 1997 CS₂₉ is a dynamically cold object with at least one satellite (Stephens & Noll 2006) and with an orbit very close to the Neptunian 7:4 MMR. The NEATM analysis of the two PACS measurements was not conclusive, only an unrealistically high η -value above 5 could connect the two fluxes. But this solution would correspond to an object with more than 1000 km diameter and an albedo below 1%. Combining the PACS 70 μm observation with two *Spitzer* measurements ($F_{24}=0.057\pm0.005$ mJy, $F_{70}=3.0\pm0.16$ mJy) confirmed that the 160 μm flux is very likely contaminated from an unknown background source. The radiometric analysis via TPM techniques (excluding now the 160 μm flux) leads to a possible diameter range between 250 and 420 km and an albedo of 6-14% for a large range of thermal inertias. The TPM analysis of the *Spitzer* observations alone are indicative of a very low thermal inertia at around $1 J m^{-2} s^{-0.5} K^{-1}$, for a $D_{eff} = 270$ km and $p_V=0.14$. Here, the fixed η approach gave 402 ± 69 km and 0.06 ± 0.02 , favouring the higher inertias above $10 J m^{-2} s^{-0.5} K^{-1}$.

² orbit parameters as FK5/J2000.0 helio. ecliptic osc. elements

(82075) 2000 YW₁₃₄ is a binary which moves on an extremely eccentric orbit and is dynamically a detached object rather than a member of the scattered disk. In a 1.5 h measurement we only obtained upper flux limits. Nevertheless, the observation (mainly the 70 μm flux) combined with the H_V magnitude in Table 2 constrain the possible diameter and albedo solutions: The target has to be smaller than about 500 km and the geometric albedo higher than 8%. Lower albedos or larger diameters would not be compatible with the non-detection at 70 μm .

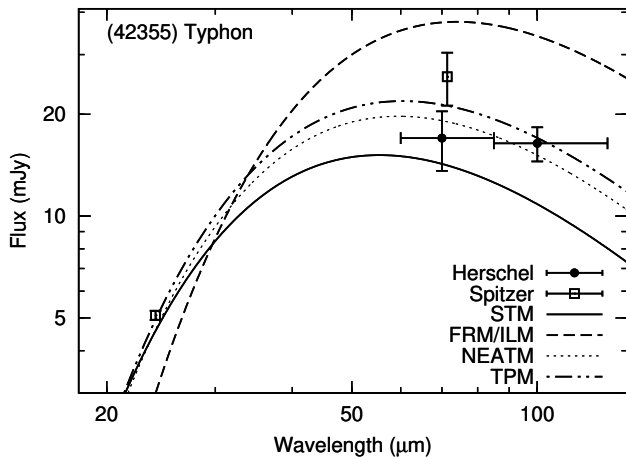


Fig. 2. The observed *Herschel* and *Spitzer* flux values for Typhon. The line-styles are the same as in Fig. 1.

(42355) Typhon is a binary Centaur on a highly eccentric orbit influenced by Uranus (Alvarez-Candal et al. 2010). We were using all *Spitzer* and PACS detections to derive radiometric properties. Via NEATM we obtained $D_{\text{eff}}=138\pm 9$ km, $p_V=0.080\pm 0.01$ for a η -value of 0.96 ± 0.08 . At a thermal inertia of $5^{+5}_{-4} \text{ J m}^{-2} \text{ s}^{-0.5} \text{ K}^{-1}$ the measured fluxes and the corresponding TPM predictions agree very well (Fig. 2). The derived effective diameter is 144 ± 10 km, the geometric albedo $p_V=0.075\pm 0.010$. The 3σ upper flux limits at 160 μm indicate that the diameter must be around 140 km or smaller, the albedo at 0.08 or larger, both values agree with the derived radiometric properties. Larger thermal inertias can be excluded due to the non-detection at 160 μm , very small thermal inertias would cause difficulties to match both *Spitzer* fluxes. Combined with the binary system mass derived by Grundy et al. (2008), we derived a bulk density of $0.66^{+0.09}_{-0.08} \text{ g cm}^{-3}$, which is slightly higher than the Grundy et al. (2008) value which was based on a single-band *Spitzer* detection (Stansberry et al. 2008).

2006 SX₃₆₈ is a Centaur on a very eccentric orbit, near the 5:4 MMR with Uranus. The PACS 70 μm detection is compatible with diameters in the range of 70-80 km and an albedo of 0.05-0.06, allowing for a wide range of thermal inertia between $0-40 \text{ J m}^{-2} \text{ s}^{-0.5} \text{ K}^{-1}$. The upper 160 μm flux limit constrains the diameter range to values below 105 km and an albedo larger than 0.03, both in agreement with the measured 70 μm -flux. The fixed η -approach gave $D_{\text{eff}}=79\pm 9$ km and $p_V=0.05\pm 0.01$.

(145480) 2005 TB₁₉₀ has a highly eccentric orbit and belongs to the detached objects. Its aphelion lies beyond 106 AU, where it may even pass through the termination shock and into the heliosheath on each orbit. Both PACS bands are beyond the emission peak for (145480) 2005 TB₁₉₀ and constrain the TPM output to an effective diameter in the range 335-410 km and an

albedo in the range 0.15-0.24. The ~ 0.3 mag uncertainty in H_V combined with lightcurve variations does not influence the diameter solution significantly, but extends the possible albedo range to 0.12-0.30. The fixed η -approach gave $D_{\text{eff}}=375\pm 45$ km and $p_V=0.19\pm 0.05$. It is the highest albedo object in our sample.

5. Conclusions

Our small and dynamically very inhomogeneous sample confirms the consistency between different model techniques and nicely agrees with *Spitzer* results (Stansberry et al. 2008) on three overlap targets. Based on the seven targets we also showed the model capabilities for multiple, dual, single or even non-detections. Models with either a beaming parameter of ~ 1.2 or thermal inertias below $25 \text{ J m}^{-2} \text{ s}^{-0.5} \text{ K}^{-1}$ explain the measured SEDs, confirming low heat conductivities at temperatures far away from the Sun. The target sizes range from diameters below 100 km to almost 1000 km. The derived geometric albedos are below 10%. Only (145480) 2005 TB₁₉₀ has an albedo above 15%, which is possibly related to its very unusual orbit located entirely outside the major planets. The derived low albedos are close to the mean value of 8% given by Stansberry et al. (2008). Albedo trends with object size, dynamic or taxonomic types are not yet visible in the small sample.

Acknowledgements. Part of this work was supported by the German *Deutsches Zentrum für Luft- und Raumfahrt*, DLR project numbers 50 OR 0903, 50 OFO 0903 and 50 OR 0904.

References

- Alvarez-Candal, A., Barucci, M. A., Merlin, F. et al. 2010, *A&A* 511, 35.
- Boehnhardt, H., Tozzi, G. P., Birkle, K. et al. 2001, *A&A* 378, 653-667.
- Bowell, E., Hapke, B., Domingue, D. et al. 1989, in *Asteroids II*, Eds. Binzel et al., Univ. of Arizona Press, 524-556.
- Davies, J. K., Green, S., McBride, N. et al. 2000, *Icarus* 146, 253-262.
- DeMeo, F. E., Fornasier, S., Barucci, A. et al. 2009, *A&A* 493, 283-290.
- Doressoundiram, A., Peixinho, N., Doucet, C. et al. 2005, *Icarus* 174, 90-104.
- Fornasier, S., Doressoundiram, A., Tozzi, G. P. et al. 2004, *A&A* 421, 353-363.
- Guilbert, A., Alvarez-Candal, A., Merlin, F. et al. 2009, *Icarus* 201, 272-283.
- Griffin, M. et al. 2010, this volume.
- Grundy, W. M., Noll, K. S., Virtanen, J. et al. 2008, *Icarus* 197, 260-268.
- Harris, A. W. 1998, *Icarus* 131, 291-301.
- Horner, J., Evans, N.W., Bailey, M. E. Asher, D. J. 2003, *MNRAS* 343, 1057.
- Horner, J., Evans, N.W. & Bailey, M. E. 2004, *MNRAS* 354, 798-810.
- Jewitt, D., Moro-Martín, A., Lacerda, P. 2009, *Astrophysics in the Next Decade*, *Astrophysics and Space Science Proc.*, Springer Netherlands, 53-102.
- Lagerros, J. S. V. 1996, *A&A* 310, 1011.
- Lagerros, J. S. V. 1997, *A&A* 325, 1226.
- Lagerros, J. S. V. 1998a, *A&A* 332, 1123.
- Lebofsky, L. A., Sykes, M. V., Tedesco, E. F. et al. 1986, *Icarus* 68, 239.
- Lebofsky, L. A. & Spencer, J. R. 1989, in *Asteroids II*, Eds. Binzel et al. Univ. of Arizona Press, 128-147.
- Lellouch et al. 2010, this volume.
- Lim, T. et al. 2010, this volume.
- Moro-Martín, A., Wyatt, M. C., Malhotra, R. et al. 2008, in *The Solar System Beyond Neptune*, Eds. Barucci et al., Univ. of Arizona Press, 465-480.
- Müller, T. G. & Lagerros, J. S. V. 1998, *A&A* 338, 340.
- Müller, T. G. & Lagerros, J. S. V. 2002, *A&A* 381, 324.
- Müller, T. G., Lellouch, E., Bönhardt, H. et al. 2009, *EM&P* 105, 209-219.
- Mueller, M., Marchis, F., Emery, J. P. et al. 2010, *Icarus* 205, 505-515.
- Morbidelli, A., Levison, H.F.; Gomes, R. 2008, in *The Solar System Beyond Neptune*, Eds. Barucci et al., Univ. of Arizona Press, 275-292.
- Perna, D., Barucci, A., Fornasier, S. et al. 2010, *A&A* 510, A53.
- Pilbratt, G. et al. 2010, this volume.
- Poglitsch, A. et al. 2010, this volume.
- Rabinowitz, D. L., Schaefer, B. E., Tourtellotte, S. W. 2007, *AJ* 133, 26-43.
- Romanishin, W. & Tegler, S. C. 1999, *Nature* 398, 129-132.
- Sheppard, S. S. & Jewitt, D. C. 2002, *AJ* 124, 1757-1775.
- Sheppard, S. S. & Jewitt, D. C. 2003, *Earth Moon and Planets*, 92, 207.
- Stansberry, J., Grundy, W., Brown, M. et al. 2008, in *The Solar System Beyond Neptune*, Eds. Barucci et al., Univ. of Arizona Press, 161-179.

Stephens, D. C. & Noll, K. S. 2006, AJ 131, 1142-1148.
Tegler, S. C., Romanishin, W., Consolmagno, G. J. 2003, ApJ 599, L49-L52.
Thirouin, A. et al. 2010, A&A, in press.
Veeder, G. J., Hanner, M. S., Matson, D. L. et al. 1989, AJ 97, 1211-1219.

-
- ¹ Max-Planck-Institut für extraterrestrische Physik (MPE), Giessenbachstrasse, 85748 Garching, Germany; e-mail: tmue11er@mpe.mpg.de
 - ² Observatoire de Paris, Laboratoire d'Etudes Spatiales et d'Instrumentation en Astrophysique (LESIA), 5 Place Jules Janssen, 92195 Meudon Cedex, France
 - ³ The University of Arizona, Tucson AZ 85721, USA
 - ⁴ Konkoly Observatory of the Hungarian Academy of Sciences, H-1525 Budapest, P.O.Box 67, Hungary
 - ⁵ Max-Planck-Institut für Sonnensystemforschung (MPS), Max-Planck-Straße 2, 37191 Katlenburg-Lindau, Germany
 - ⁶ Observatoire de la Côte d'Azur, laboratoire Cassiopée B.P. 4229; 06304 NICE Cedex 4; France
 - ⁷ Laboratoire d'Astrophysique de Marseille, CNRS & Université de Provence, 38 rue Frédéric Joliot-Curie, 13388 Marseille cedex 13, France
 - ⁸ Instituto de Astrofísica de Andalucía (CSIC) C/ Camino Bajo de Huétor, 50, 18008 Granada, Spain
 - ⁹ Observatoire de Paris, Laboratoire d'Etudes Spatiales et d'Instrumentation en Astrophysique (LESIA), University of Paris 7 “Denis Diderot”, 4 rue Elsa Morante, 75205 Paris Cedex
 - ¹⁰ Deutsches Zentrum für Luft- und Raumfahrt, Berlin-Adlershof, Rutherfordstraße 2, 12489 Berlin-Adlershof, Germany
 - ¹¹ Department of Physics and Astronomy, Science Laboratories, University of Durham, South Road, Durham, DH1 3LE, United Kingdom
 - ¹² Newton Fellow of the Royal Society, Astrophysics Research Centre, Physics Building, Queen's University, Belfast, County Antrim, BT7 1NN, UK
 - ¹³ Space Science and Technology Department, Science and Technology Facilities Council, Rutherford Appleton Laboratory, Harwell Science and Innovation Campus, Didcot, Oxon UK, OX11 0QX
 - ¹⁴ Northern Arizona University, Department of Physics & Astronomy, PO Box 6010, Flagstaff, AZ 86011, USA
 - ¹⁵ INAF-Osservatorio Astronomico di Roma, Via di Frascati, 33, 00040 Monte Porzio Catone, Italy
 - ¹⁶ ESO, Karl-Schwarzschild-Str. 2, 85748 Garching, Germany
 - ¹⁷ IMCCE/Observatoire de Paris, CNRS, 77 Av. Denfert-Rochereau, 75014 Paris, France
 - ¹⁸ Herschel Science Centre (HSC), European Space Agency (ESA), European Space Astronomy Centre (ESAC), Camino bajo del Castillo, s/n, Urbanizacion Villafranca del Castillo, Villanueva de la Cañada, 28692 Madrid, Spain
 - ¹⁹ Universität Bern, Hochschulstrasse 4, CH-3012 Bern, Switzerland